

Super-Resolution Reconstruction in MRI: Better Images Faster?

Esben Plenge^{1,*}, Dirk H. J. Poot¹, Monique Bernsen²,
Gyula Kotek², Gavin Houston², Piotr Wielopolski²,
Louise van der Weerd³, Wiro J. Niessen^{1,4}, Erik Meijering¹

¹ Biomedical Imaging Group Rotterdam, Departments of Medical Informatics and Radiology,
Erasmus MC – University Medical Center Rotterdam, Rotterdam, The Netherlands

² Department of Radiology, Erasmus MC – University Medical Center Rotterdam, Rotterdam, The Netherlands

³ Departments of Radiology & Human Genetics, Leiden University Medical Center, Leiden, The Netherlands

⁴ Quantitative Imaging Group, Department of Imaging Science & Technology, Faculty of Applied Sciences,
Delft University of Technology, Delft, The Netherlands

ABSTRACT

Improving the resolution in magnetic resonance imaging (MRI) is always done at the expense of either the signal-to-noise ratio (SNR) or the acquisition time. This study investigates whether so-called super-resolution reconstruction (SRR) is an advantageous alternative to direct high-resolution (HR) acquisition in terms of the SNR and acquisition time trade-offs. An experimental framework was designed to accommodate the comparison of SRR images with direct high-resolution acquisitions with respect to these trade-offs. The framework consisted, on one side, of an image acquisition scheme, based on theoretical relations between resolution, SNR, and acquisition time, and, on the other side, of a protocol for reconstructing SRR images from a varying number of acquired low-resolution (LR) images. The quantitative experiments involved a physical phantom containing structures of known dimensions. Images reconstructed by three SRR methods, one based on iterative back-projection and two on regularized least squares, were quantitatively and qualitatively compared with direct HR acquisitions. To visually validate the quantitative evaluations, qualitative experiments were performed, in which images of three different subjects (a phantom, an ex-vivo rat knee, and a post-mortem mouse) were acquired with different MRI scanners. The quantitative results indicate that for long acquisition times, when multiple acquisitions are averaged to improve SNR, SRR can achieve better resolution at better SNR than direct HR acquisitions.

Keywords: Magnetic resonance imaging, super-resolution, reconstruction, image quality

1. PURPOSE

Super-resolution reconstruction (SRR) is the process of producing a high-resolution (HR) image from a sequence of low-resolution (LR) images, where each LR image transforms and samples the HR scene in a distinct fashion, see Fig. 1. The idea was first introduced in the 1980s¹ and has since grown into a research field of its own. The first example of SRR applied to MRI was described in a 1997 patent.² While SRR in MRI is a developing field, and encouraging results have been published showing its potential in resolution enhancement,^{3–5} a major concern from the MRI community is whether SRR has any advantage over direct HR acquisition when SNR and acquisition times are taken into account. In this study, we present a framework for experimentally comparing the performance of SRR methods with that of direct acquisition. We show the efficacy of the framework on three SRR methods, chosen from classical and more recent SRR MRI papers.

2. THEORY

2.1 Super-Resolution in MRI

There is consensus that super-resolution in MRI is not achievable in-plane, nor in true 3D acquisitions, since the Fourier encoding scheme excludes aliasing in frequency and phase encoding directions.⁶ Often, however, when image contrast requirements yield long repetition times (as in e.g. T_2 -weighted images), it will be significantly faster to acquire 2D slice stacks than to acquire true 3D volumes due to the possibility acquiring the slices in an interleaved fashion. In 2D slice

*Corresponding author (e.plenge@erasmusmc.nl)

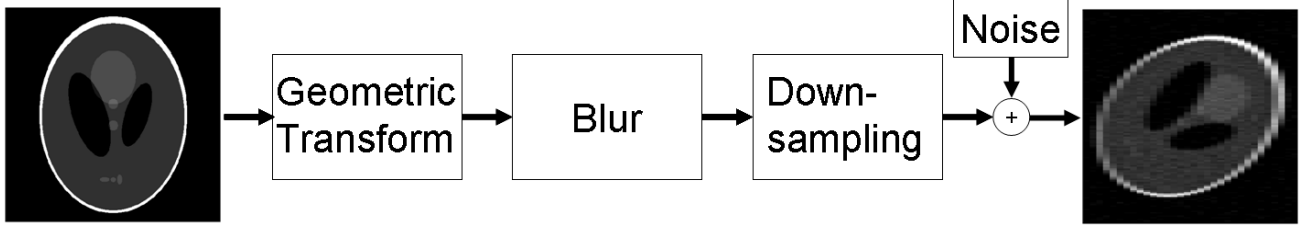


Figure 1: Illustration of the imaging model applied in super-resolution reconstruction. Low-resolution images (right) are the result of geometric transformation, blurring, and down-sampling of high-resolution images (left), and the addition of noise.

stacks, the individual slices are Fourier encoded and the frequency content is thus inherently limited in-plane. In the through-plane direction, however, there are no theoretical limitations on the frequency spectrum, and aliased frequencies may potentially be recovered. The amount of aliasing depends on the shape of the slice profile. This profile is ideally a rect function but in practice, since it is the Fourier transform of the slice excitation radio-frequency pulse, which is a truncated sinc, it becomes only an approximation of the rect function.

Thinner slices require more slices to acquire a given volume, and acquisition time scales approximately linearly with the number of slices. SNR scales linearly with slice thickness, and, by averaging multiple acquisitions, SNR scales with a factor $\sqrt{T_{\text{acq}}}$, where T_{acq} is the acquisition time. This relationship is illustrated in Fig. ??.

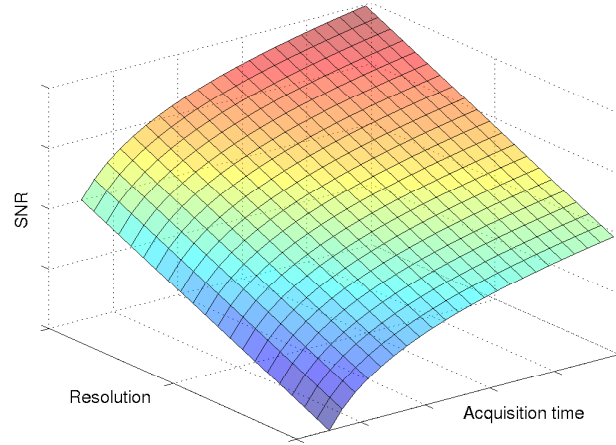


Figure 2: Illustration of the MRI trade-offs between resolution, SNR and acquisition time. Any conventional MRI acquisition is located on the plotted surface.

Thus, in conventional 2D MRI, if hardware, imaging sequence, and field-of-view (FOV) are fixed, the relationship between slice thickness h , SNR, and acquisition time, T_{acq} is given by

$$\text{SNR} \propto h \sqrt{T_{\text{acq}}}. \quad (1)$$

2.2 The Super-Resolution Methodology

The MRI acquisition process can be modeled by a linear system \mathbf{A} encompassing a geometric transformation, blur and sampling operators, and a Gaussian noise model.⁷ The k^{th} acquisition in a series of LR images can thus be described by

$$\mathbf{y}_k = \mathbf{A}_k \mathbf{x} + \mathbf{n}_k, \quad (2)$$

where \mathbf{x} is the HR scene to be reconstructed.

SRR is an inverse problem and involves recovering \mathbf{x} given the \mathbf{y}_k and \mathbf{A}_k . The problem can be formulated as an ordinary least squares (LS) problem,

$$\mathbf{x} = \underset{\mathbf{x}}{\operatorname{argmin}} \sum_{k=1}^N \|\mathbf{y}_k - \mathbf{A}_k \mathbf{x}\|^2. \quad (3)$$

Using additional prior knowledge about the solution, e.g. that it is smooth, Eq. (3) generalizes to

$$\mathbf{x} = \underset{\mathbf{x}}{\operatorname{argmin}} \sum_{k=1}^N \|\mathbf{y}_k - \mathbf{A}_k \mathbf{x}\|^2 + \lambda \mathbf{C} , \quad (4)$$

where \mathbf{C} is a regularization term formalizing the prior, and λ is a scalar weight. Eq. (4) is also known as the *regularized* LS problem.

A direct solution of Eqs. (3) and (4) is generally infeasible. Instead, iterative methods are usually applied to approximate the solution. To validate the efficacy of our evaluation framework, we have implemented three SRR methods. One, is the classical iterative back-projection method (IBP),^{3,8} that solves Eq. (3). The two other methods (TIK and LASR), both solve Eq. (4) using regularized Tikhonov least-squares solvers, where the L_2 -norm of the second-order derivative of the HR reconstruction is used as regularization term:

$$\mathbf{C} = \|\nabla^2 \mathbf{x}\|^2 = \left(\frac{\partial^2 \mathbf{x}}{\partial r_1^2} \right)^2 + \left(\frac{\partial^2 \mathbf{x}}{\partial r_2^2} \right)^2 + \left(\frac{\partial^2 \mathbf{x}}{\partial r_3^2} \right)^2 . \quad (5)$$

Here r_i is the spatial dimension over which the partial derivative is taken. In both the TIK and LASR methods, the regularized LS problem of Eq. [4] was solved with the conjugate gradient method and the transforms in \mathbf{A} and \mathbf{A}^T were implemented using bilinear interpolation and an aliasing-reducing interpolation scheme,⁹ respectively.

The experiments with TIK and LASR in this study, were performed with little regularization ($\lambda = 0.004$). These values were found by experimenting with a range of λ -values and qualitatively determining the best result.

3. METHODS

To evaluate whether SRR methods can decrease the slice thickness of MR images at better SNR and timing trade-offs than direct HR acquisition, we devised an evaluation framework, using the following relations (illustrated in Fig. ??): 1) for a fixed FOV, the acquisition time scales inversely with slice thickness, 2) the SNR scales linearly with slice thickness, 3) the SNR scales with the square root of the acquisition time (Eq. (1)). Also, for a given imaging sequence, FOV, and resolution, the SNR is improved by averaging multiple acquisitions, so T scales linearly with the number of averaged acquisitions.

To quantitatively evaluate the performance of the SRR methods we used MRI images of a Varian phantom. A low-resolution (LR) dataset consisting of 24 2D slice stacks of $1.0 \times 1.0 \times 4.0$ mm resolution was acquired while rotating the FOV of the stacks around the phase encoding axis in uniform increments of approximately $180/24$ degrees. The rotated acquisition scheme, introduced by Shilling et al. in,¹⁰ was chosen over simply shifting the slice stacks in the slice selection by sub-pixel increments. The latter approach corresponds to simply increasing the sampling density of the object after convolving it with the slice selection profile, thus merely over-sampling the signal. By rotating the slice selection direction between each LR image, the narrow bandlimit of that direction will rotate as well. Thus each image is oriented in a different direction of the 3D frequency spectrum of the imaged object. In this case, the LR data set will contain high spatial frequency content in all three dimensions.

Eight subsets were picked from the 24 slice stacks containing $n = 1, 2, 3, 4, 6, 8, 12,$ and 24 stacks, respectively. Each subset was selected such that the rotational increments among its slice stacks were approximately equal. If we denote the acquisition time of one LR image by T_{LR} , each subset thus had an acquisition time of $n T_{LR}$. Reconstruction of 1 mm isotropic resolution images from the eight LR subsets allowed evaluating resolution and SNR as functions of the acquisition time. In addition, we implemented a simple bilinear interpolation method (INT) for reference.

For comparison, isotropic HR reference images were acquired directly at 1 mm resolution. Because these images had a resolution in the slice selection direction four times higher than the LR images, they required an acquisition time of $4 T_{LR}$ each. For a given imaging sequence, and given contrast and resolution settings, conventional MRI can improve the image quality only by averaging multiple images. Imaging time increases linearly with the number of averaged images. This way, the quality of direct acquisitions (DAC) could be evaluated at time points that were multiples of $4 T_{LR}$, covering the same total time range as the LR images used for reconstruction, see Fig. 3.

Resolution (in millimeters) was measured in each image as the average width of 20 edge profiles.^{3,10} The SNR was computed by dividing the mean of a high-intensity foreground region with the standard deviation of a background region.

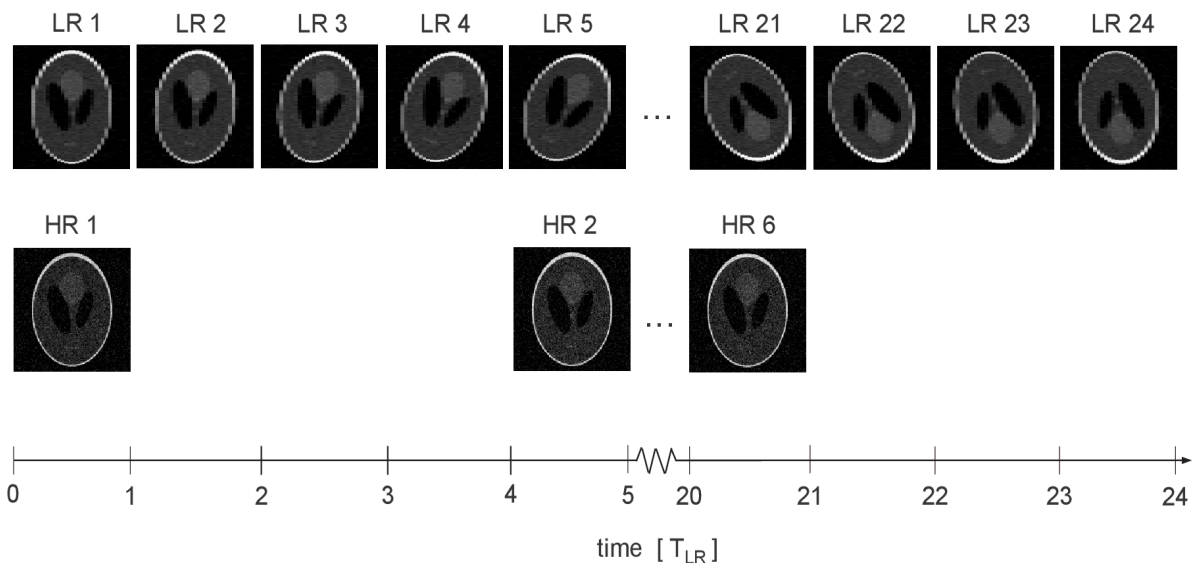


Figure 3: Illustration of the simulation and acquisition scheme of the quantitative experiments. Upper row: 24 LR images are simulated/acquired while rotating the FOV around the phase-encoding axis in increments of $24/180$ degrees. Lower row: Six HR images of 4 times thinner slices and 4 times longer acquisition time than the LR images are simulated/acquired, enabling post-acquisition production of multiple averages images. Note that the image planes shown (both LR and HR) are spanned by the frequency encoding and slice selection directions. The unit of the time axis is T_{LR} , the acquisition time of a single LR image.

To qualitatively validate the quantitative experiments described above, additional LR data sets were acquired: one of the Varian phantom, one of a full-body post-mortem mouse, and one of an ex-vivo rat-knee.

4. RESULTS

The results of the quantitative evaluations are summarized in Fig. 4. The figure shows the resolution and SNR of the reconstructions versus the acquisition time for the three SRR methods, bilinear interpolation, and direct acquisition. For reference, the graphs also include the theoretical curves (THEO) of isotropic 1.2, 1.3, and 1.4 mm resolution images. It can be observed how the TIK reconstructions surpass the measured resolution of the DAC images around $15 T_{LR}$ while its SNR at that point is more than 6 dB higher than that of the DAC images. Furthermore, it is seen how TIK reconstructions reach a resolution of 1.2 mm already at $5 T_{LR}$. For acquisition times beyond $12 T_{LR}$, the measured resolution of IBP reconstructions is around 1.2 mm, while the SNR for this method at $12 T_{LR}$ is 3.0 dB higher than that of a direct acquisition of 1.2 mm isotropic resolution. At $24 T_{LR}$, this difference is even 4.8 dB. From $4 T_{LR}$ to $8 T_{LR}$, the IBP reconstructions reach a measured resolution of approximately 1.3 mm, while the corresponding SNRs are only slightly (0.5-0.8 dB) higher than that of the theoretical 1.3 mm resolution image.

The qualitative experiments using the Varian phantom (Fig. 5) show the improvement in resolution with SRR using 12 LR images. The resolution of directly acquired HR images is approached by the reconstruction. In Fig. 6 it is seen how the resolution of reconstructed images of a post-mortem mouse increases with the number of LR images used for reconstruction. Finally, in Fig. 7, the effect of SRR for reconstructing isotropic voxels can be appreciated. In this experiment the slice thickness of the acquisitions was at the lower limit of the scan system. It is seen how the resolution in the slice selection direction of the reconstructions exceeds the maximum resolution of the system in that direction.

5. DISCUSSION AND CONCLUSION

While the performance of SRR compared with direct acquisitions has been studied before,³ no framework that allows thorough analysis of the relations between resolution, SNR, and acquisition time has previously been described in the literature, and therefore the net practical advantage of using SRR has so far remained unclear. The presented evaluation framework allows such investigation.

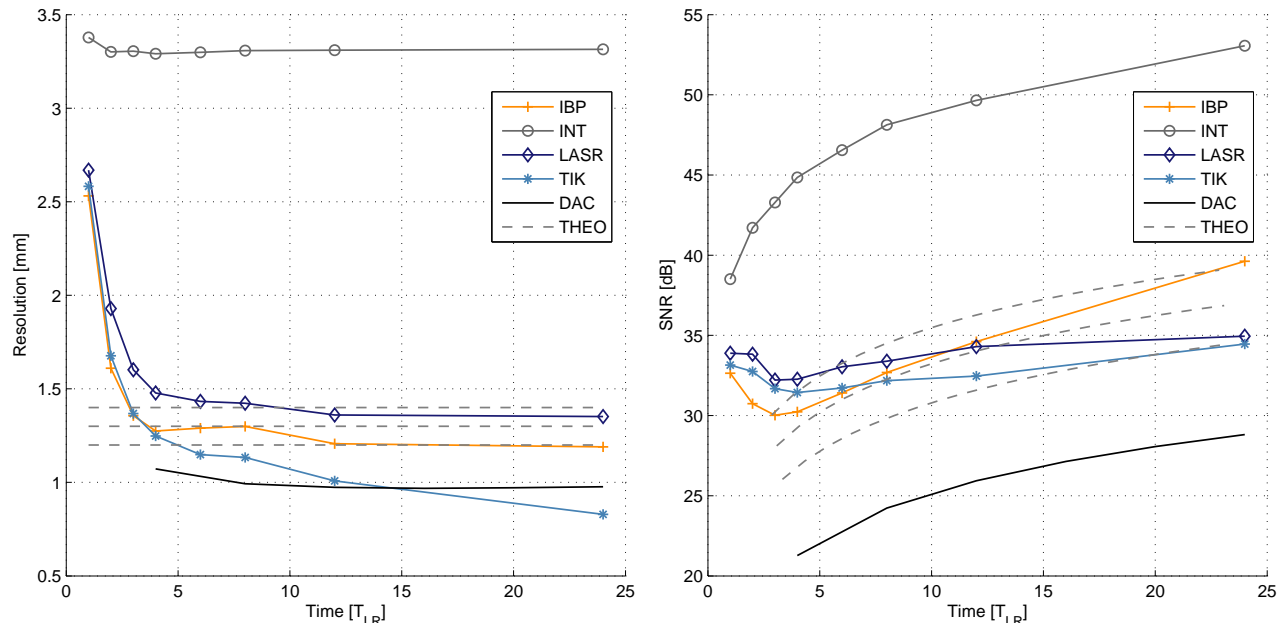


Figure 4: The resolution (left) and SNR (right) of reconstructions by the three SRR methods (IBP, LASR, TIK) and bilinear interpolation (INT) as a function of acquisition time is compared to direct HR imaging (DAC) at 1 mm resolution and theoretical images (THEO) of resolution 1.2, 1.3, 1.4 mm (from lower to upper dashed curves) for the MRI data of the Varian phantom. The unit of time along the x-axis is T_{LR} (the time required to acquire one LR image).

While the quantitative evaluation of the TIK method looks as if the reconstructions surpass the resolution of the direct acquisition, this is not confirmed by qualitative experiments. In these, the direct HR in-plane view of the structure of interest consistently looks better than the reconstructed images. The discrepancy between the quantitative and the qualitative results may be explained by the used edge width measure, which is sensitive to overshoots, and we have noticed that the TIK algorithm has the tendency to produce such effects.

For the IBP algorithms, however, no overshoot artifact were observed, and we believe that the quantitative results are valid. On this basis we conclude that SRR is indeed able to improve the trade-off compared to conventional MRI. Another point that can be seen from our results, in particular Fig. 7, is that SRR is capable of improving the resolution in the slice selection direction beyond the slice thickness limits imposed by the scanner system.

6. ACKNOWLEDGEMENTS

The authors would like to thank Mark Halberstadt (Erasmus MC) and Ernst Suidgeest (Leiden UMC) for assistance in MRI acquisition, and Gerben van Buul (Erasmus MC) for the ex-vivo knee sample. The work presented in this paper has been funded by Medical Delta (HST-Klein project) and by the European Commission in the Seventh Framework Programme (ENCITE project).

REFERENCES

- [1] Tsai, R. Y. and Huang, T. S., “Multi-frame image restoration and registration,” in [*Advances in Computer Vision and Image Processing*], 1, 317–339, JAI Press Inc. (1984).
- [2] Fiat, D., “Method of enhancing an MRI signal,” (2001). United States Patent 6294914.
- [3] Greenspan, H., Oz, G., Kiryati, N., and Peled, S., “MRI inter-slice reconstruction using super-resolution,” *Magn Reson Imaging* 20(5), 437–446 (2002).
- [4] Greenspan, H., “Super-resolution in medical imaging,” *Comput J* 52(1), 43–63 (2009).
- [5] Gholipour, A., Estroff, J., and Warfield, S., “Robust super-resolution volume reconstruction from slice acquisitions: Application to fetal brain MRI,” *IEEE Trans Med Imaging* 29(10), 1739–1758 (2010).
- [6] Scheffler, K., “Superresolution in MRI?,” *Magn Reson Med* 48(2), 408; author reply 409 (2002).

- [7] Gudbjartsson, H. and Patz, S., “The Rician distribution of noisy MRI data.,” *Magn Reson Med* **34**(6), 910–914 (1995).
- [8] Irani, M. and Peleg, S., “Improving resolution by image registration,” *CVGIP: Graph Models Image Process* **53**(3), 231–239 (1991).
- [9] Poot, D. H. J., Van Meir, V., and Sijbers, J., “General and efficient super-resolution method for multi-slice MRI,” in [*Proceedings of the 13th International Conference on Medical Image Computing and Computer-Assisted Intervention: Part I*], 615–622, Springer-Verlag, Berlin (2010).
- [10] Shilling, R. Z., Robbie, T. Q., Bailloeu, T., Mewes, K., Mersereau, R. M., and Brummer, M. E., “A super-resolution framework for 3-D high-resolution and high-contrast imaging using 2-D multislice MRI.,” *IEEE Trans Med Imaging* **28**(5), 633–644 (2009).

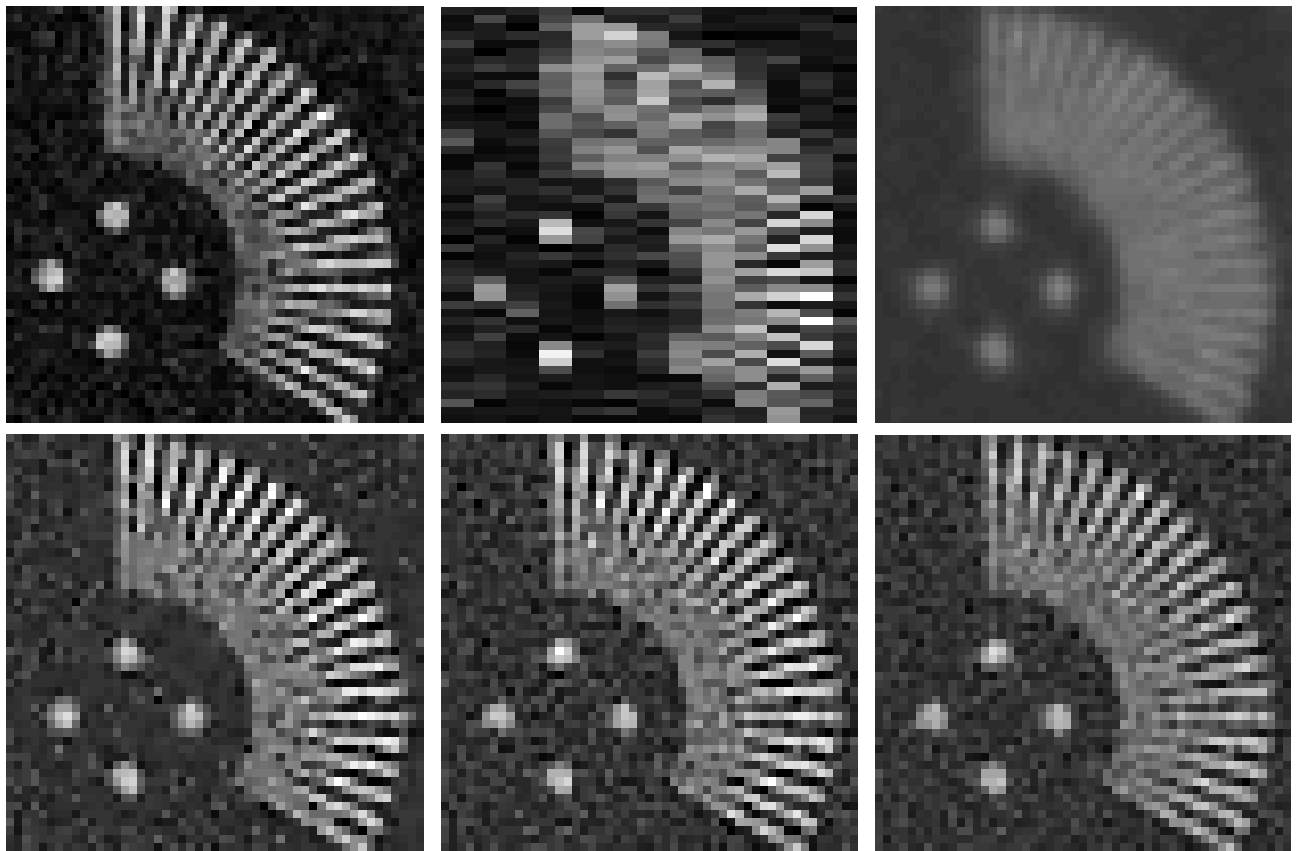


Figure 5: Visual impression of the performance of the SRR methods on the Varian phantom data. The panels show (in scan-line order) a structure of interest in the: HR plane of a direct acquisition, LR plane, and as reconstructed by INT, IBP, TIK, and LASR. The reconstructions are based on 12 LR images. The intensities of each image have been scaled according to the mean value of a homogeneous high-intensity region in the image.

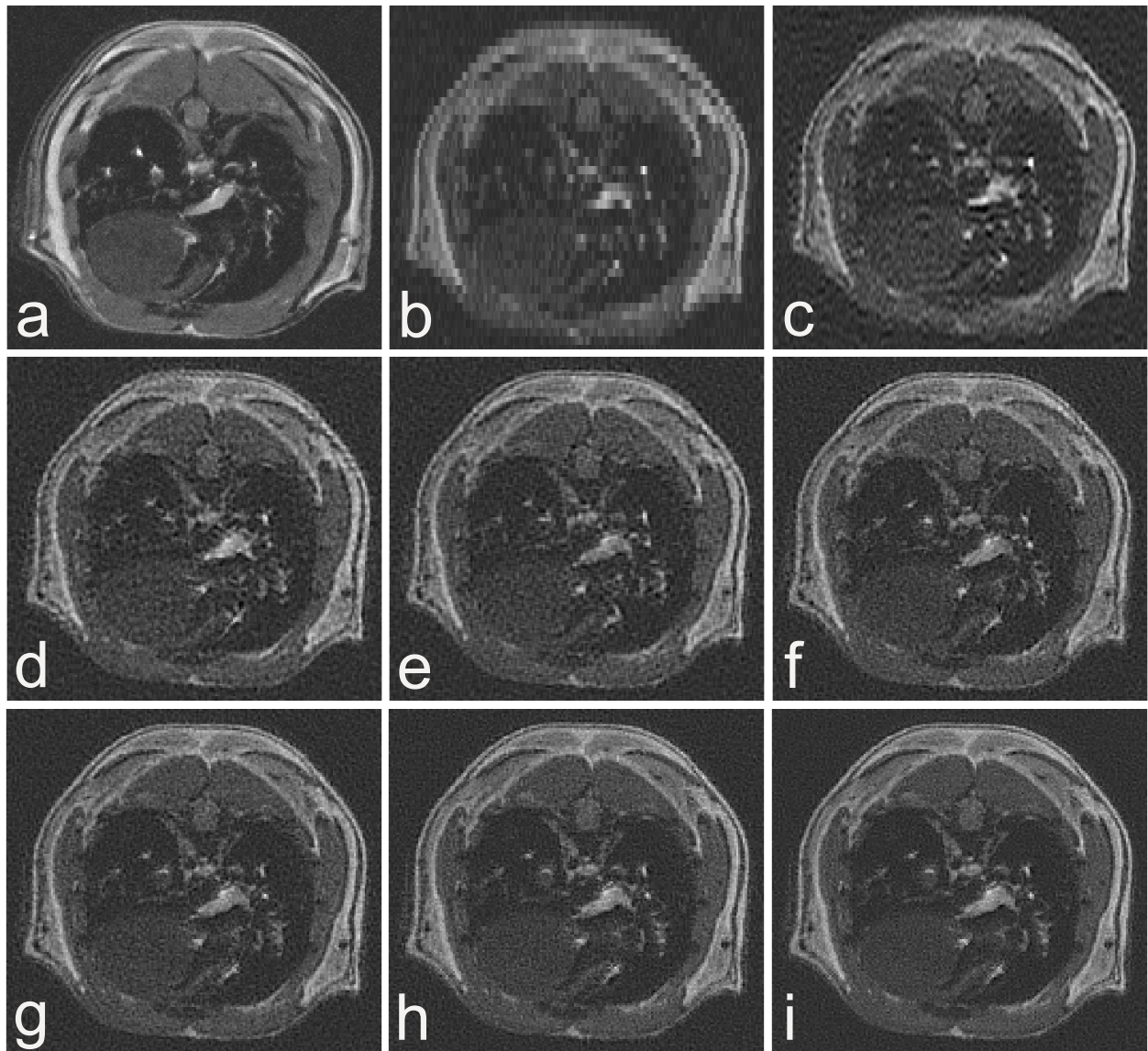


Figure 6: Axial slices of the full-body mouse scan. The images show: (a) a slice from a direct acquisition with thick slices but high resolution in the plane shown, (b) one of the LR acquisitions, and the results of TIK using (c) 2, (d) 3, (e) 4, (f) 6, (g) 8, (h) 12, and (i) 24 LR images.

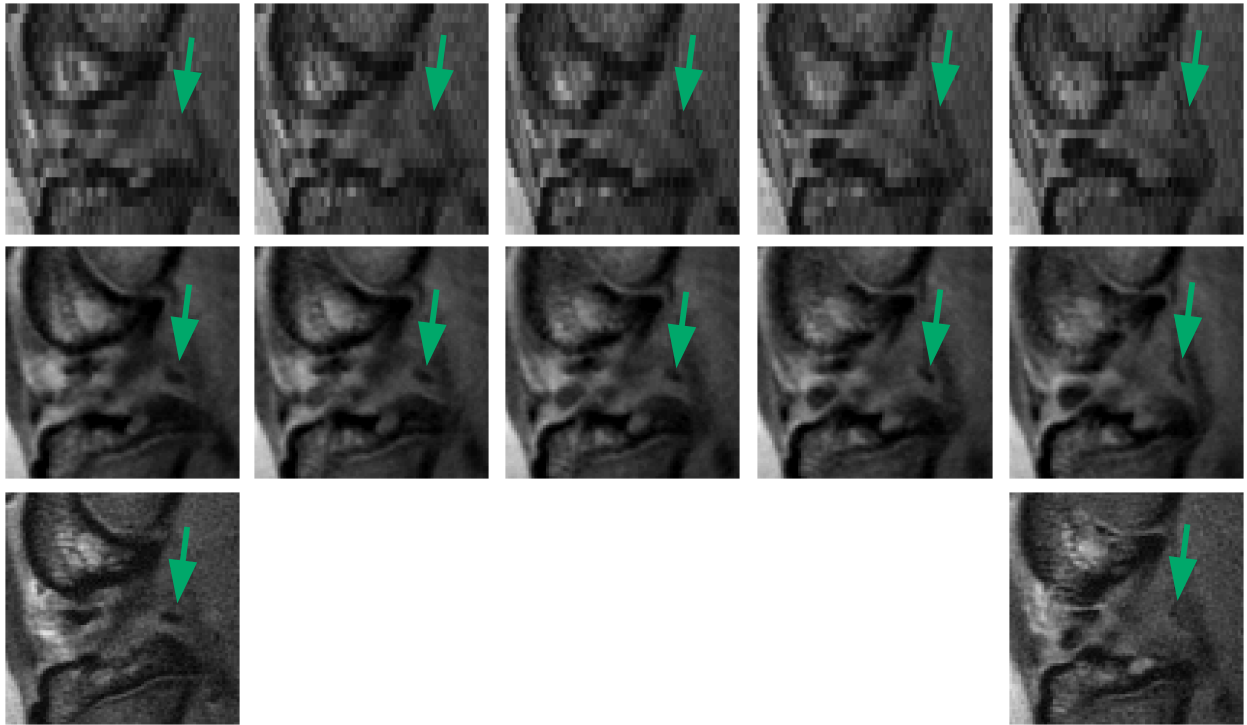


Figure 7: Potential of SRR demonstrated on ex-vivo data of a rat knee with SPIO-labeled cells (at arrows). Top row: a sequence of consecutive reformatted 2D views of anisotropic LR acquisition with the slice selection direction along the vertical axis. Middle row: corresponding SRR slices, reconstructed using 12 LR images and the TIK method. Bottom row: two slices of anisotropic reference acquisition with target resolution in the plane reconstructed above. The three sequences all cover approximately the same spatial volume.